0026-895X/93/04681-08$03.00/0

MOLECULAR PHARMACOLOGY, 44:681-688

ACCELERATED COMMUNICATION

Structure and Properties of ω-Agatoxin IVB, a New Antagonist of P-Type Calcium Channels

MICHAEL E. ADAMS, ISABELLE M. MINTZ, MICHAEL D. REILY, VENKATARAMAN THANABAL, and BRUCE P. BEAN

Departments of Entomology and Neuroscience, University of California, Riverside, California 92521 (M.E.A.), Department of Chemistry, Parke-Davis Pharmaceutical Research Division, Warner Lambert Co., Ann Arbor, Michigan 48105 (M.D.R., V.T.), and Department of Neurobiology, Harvard Medical School, Boston, Massachusetts 02115 (I.M.M., B.P.B.)

Received June 21, 1993; Accepted July 23, 1993

SUMMARY

A new peptide antagonist of voltage-activated calcium channels was purified from venom of the funnel web spider, *Agelenopsis aperta*. This 48-amino acid peptide, ω-agatoxin (ω-Aga)-IVB, was found to be a potent (K_d, ~3 nM) blocker of P-type calcium channels in rat cerebellar Purkinje neurons but had no activity against T-type, L-type, or N-type calcium channels in a variety of neurons. The calcium channel-blocking properties of ω-Aga-IVB were similar to those of another toxin, ω-Aga-IVA, which has 71% amino acid identity with ω-Aga-IVB. The 10-fold greater abundance of ω-Aga-IVB in venom allowed structural studies using NMR spectroscopy. The three-dimensional structure derived from NMR data resulted in a proposed disulfide bond configuration for the peptide. Although ω-Aga-IVB has fewer basic and more acidic residues than does ω-Aga-IVA, the two toxins show conservation of positively charged residues in a mid-peptide region that is predicted to form one face of the ω-Aga-IVB molecule. This region may be crucial for high affinity binding to the P-type calcium channel. In contrast, the amino termini of the two toxins have different charges and seem unlikely to be involved in binding to the channel.

Venomous animals use complex cocktails of toxins for prey capture or for defense. Many of the toxins contained in venoms are targeted to ion channels and receptors and are proving to be useful pharmacological tools (1–4). Indeed, unique toxin binding sites on ion channels have been the basis for pharmacological classification of some types of ion channels, including voltage-activated calcium channels.

Multiple types of voltage-activated calcium channels have been found in mammalian neurons by voltage-clamp studies, and differential sensitivity to drugs and toxins has been crucial in distinguishing these channel types (5–7). Multiple types of calcium channels also have been identified by cloning of brain cDNA, and there is now great interest in correlating cloned calcium channels with those identified electrophysiologically (6–8). So far, excellent correlations have been established for two classes of channels, based in large part on channel pharmacology. Dihydropyridine drugs such as nifedipine, nimodipine, and Bay K8644 are highly selective for L-type channels, as expressed normally in neurons (9, 10) or as expressed from cloned cDNA (11). ω-CgTX, a peptide toxin from the venom of the cone snail *Conus geographus*, is highly selective for a distinct class of N-type calcium channels, as expressed both in neurons (10, 12) and from cloned cDNA (13).

A third type of high-threshold calcium channel, the P-type channel, was originally identified in rat cerebellar Purkinje neurons and was found to be insensitive to both dihydropyridines and ω-CgTX (14, 15). A peptide toxin from venom of the spider *Agelenopsis aperta*, ω-Aga-IVA, has been identified as a potent selective blocker of P-type calcium channels (16, 17). Based on sensitivity to ω-Aga-IVA, fractions of calcium current carried by P-type channels were identified in a variety of central and peripheral neurons. Our understanding of P-type calcium channels is still quite limited, however, especially because there is no clear identification with any of the cloned calcium channels (see Refs. 6 and 7). Further pharmacological characterization of P-type channels should be helpful in establishing this link.

This work was supported by United States Public Health Service Grants NS24472 (to M.E.A.) and NS02253 (to B.P.B) and by Biomedical Research Support Group Grant 2 S07 RR07010-22 to the University of California, Riverside, Biotechnology Facility.

ABBREVIATIONS: ω-CgTX, ω-conotoxin GVIA; ω-Aga, ω-agatoxin; NOESY, nuclear Overhauser spectroscopy; MS, mass spectrometry; ES, electrospray; FAB, fast atom bombardment; NOE, nuclear Overhauser effect; TFA, trifluoroacetic acid; DRG, dorsal root ganglion; RMS, root mean square; HEPES, 4-(2-hydroxyethyl)-1-piperazineethanesulfonic acid; EGTA, ethylene glycol bis(β-aminoethyl ether)-*N*,*N*,*N*′,*N*′-tetraacetic acid.

We have searched for additional toxins in *A. aperta* venom that may have activity against P-type calcium channels. Here we describe a new toxin, designated ω-Aga-IVB, which we found to be a highly potent blocker of P-type calcium channels in rat neurons. The amino acid sequence of ω-Aga-IVB has substantial similarity to that of ω-Aga-IVA, and its selectivity for particular types of calcium channels was also found to be similar to that of ω-Aga-IVA. Because ω-Aga-IVB is present in venom at a 10-fold higher concentration, compared with ω-Aga-IVA, it has been possible to isolate sufficient quantities for a detailed analysis of its three-dimensional structure.

Materials and Methods

Toxin isolation and sequencing. ω-Aga-IVB was purified from crude *A. aperta* venom using high performance liquid chromatography protocols based on those described previously (4, 16). Whole venom was fractionated on a Brownlee C_8 wide-pore analytical column (4.6 × 150 mm) with a linear gradient of aqueous acetonitrile in constant 0.1% TFA, at a flow rate of 1.0 ml/min. The peak labeled IVB in Fig. 1A was purified further using a Brownlee C_8 column and a linear gradient of *n*-propyl alcohol/water (0.33%/min) in constant 1% TFA. A third high performance liquid chromatography step made use of a Vydac wide-pore C_{18} analytical column and a linear gradient of aqueous acetonitrile in constant 0.1% TFA.

Amino acid composition and sequencing analyses were performed at the University of California, Riverside, Biotechnology Instrumentation Facility, using methods described previously (4, 16, 18). ES- and FAB-MS were performed at the Beckman Research Institute, City of Hope Hospital (Duarte, CA), according to previously reported methods (16).

Synaptosomes. Synaptosomes were prepared from whole rat brains (minus brainstem) of 14–20-day-old Sprague-Dawley rats as described (16), with the following modifications. Brain homogenates were centrifuged at low speed (3000 × *g* for 10 min) to yield a P1 pellet. After the pellet was washed, supernatants were pooled and centrifuged a second time, at 12,500 × *g* for 20 min, to obtain a P2 pellet. Instead of purifying a synaptosomal fraction from the P2 pellet as done previously (16), we simply resuspended the P2 pellet and used it directly for $^{45}Ca^{2+}$ flux experiments. This less cumbersome approach was adopted because data obtained with the resuspended P2 pellet were identical to those obtained with the purified synaptosomal fraction. The resuspended P2 pellet was incubated with toxin fractions (10–20 min) at 4° and then warmed to 30° over 10 min before depolarization with 40 mM KCl. $^{45}Ca^{2+}$ influx was terminated at 5 sec by addition of excess wash solution, and the solution was rapidly filtered using a Skatron cell harvester. Radioactivity trapped on the filters was used as a measure of Ca^{2+} entry into synaptosomes; counts from low-potassium tubes were subtracted from those from high-potassium tubes to obtain the voltage-sensitive fraction of $^{45}Ca^{2+}$ entry.

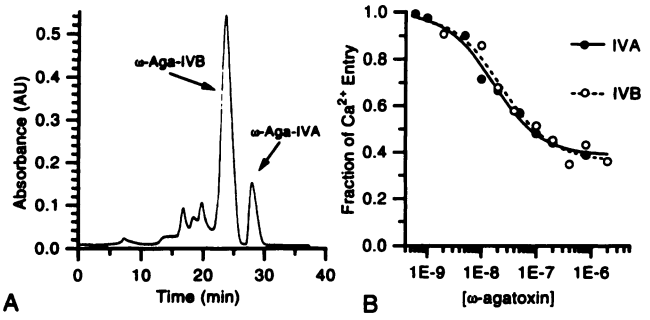


```
C   ω-Aga-IVB
    EDNCIAEDYG KCTWGGTKCC RGRPCRCSMI GTNCECTPRL IMEGLSFA
    --    --   +      +   + + +          -   +    -
    +++   +-   + +        + +              - + +    -
    KKKCIAKDYG RCKWGGTPCC RGRGCICSIM GTNCECKPRL IMEGLGLA
    ω-Aga-IVA
```

Fig. 1. Isolation and sequence analysis of ω-Aga-IVB. A, Liquid chromatography elution profile of ω-Aga-IVB (*IVB*) and ω-Aga-IVA (*IVA*) after the first high performance liquid chromatography step. Venom was fractionated on a Brownlee C_8 wide-pore analytical column (4.6 × 150 mm) with a linear gradient of aqueous acetonitrile in constant 0.1% TFA, at a flow rate of 1.0 ml/min. B, Block of potassium-stimulated $^{45}Ca^{2+}$ entry into rat brain synaptosomes by ω-Aga-IVB and ω-Aga-IVA. C, Amino acid sequence of ω-Aga-IVB and alignment with ω-Aga-IVA.

Electrophysiology. Whole-cell recordings were made from acutely dissociated rat neurons as described previously (17). Pipettes (1–3 MΩ resistance) were filled with an internal solution of (in mM) 108 cesium methanesulfonate, 4 $MgCl_2$, 9 EGTA, 9 HEPES, 4 Mg-ATP, 14 creatine phosphate (Tris salt), and 0.3 GTP (Tris salt), pH 7.4. After whole-cell recording was established with the cells in Tyrode's solution (150 mM NaCl, 4 mM KCl, 2 mM $CaCl_2$, 2 mM $MgCl_2$, 10 mM glucose, 10 mM HEPES, pH 7.4 with NaOH), cells were transferred to a 50–60-μl minichamber, where steady toxin applications could be made using minimal amounts of material. The external solution in the minichamber was 5 mM $BaCl_2$, 160 mM tetraethylammonium chloride, 10 mM HEPES, pH 7.4 with tetraethylammonium hydroxide. Cytochrome *c* (1 mg/ml) was included in all external solutions to prevent loss of toxin to the walls of the containers. Toxins and drugs were added to the minichamber from 10-fold more concentrated stock solutions prepared in the external solution. Recovery from toxin block was monitored during continuous washing of the minichamber using a gravity-driven perfusion system. Synthetic ω-CgTx was purchased from Peninsula Laboratories. Bay K8644 and nimodipine were gifts from Dr. Alexander Scriabine, Miles Laboratories (West Haven CT).

Voltage pulses were generated and currents were digitized using the Basic FastLab system (INDEC Systems, Sunnyvale, CA). Currents were filtered at 3–10 kHz (−3 dB, four-pole low-pass Bessel filter) and digitized every 20–100 μsec. Reported potentials were corrected for a liquid junction potential of −10 mV between the internal solution and the Tyrode's solution in which the pipette current was zeroed before sealing onto a cell. Calcium channel currents were corrected for leak and capacitative currents by subtraction of an appropriately scaled current elicited by a 10-mV hyperpolarization. Statistics are given as mean ± standard error. All experiments were done at 21–24°.

NMR spectroscopy. NMR spectra were recorded at 500 or 600 MHz on 4 or 8 mg of ω-Aga-IVB dissolved in 0.5 ml of either 10% ^2H_2O/90% H_2O or 100% ^2H_2O at pH 2.6. Total correlated spectroscopy (19) spectra were acquired with a 60-msec 7-kHz MLEV-17 (20) spin-lock field. NOESY (21) spectra were acquired with a mixing time of 80, 160, or 250 msec, with presaturation of the H_2O signal during the mixing time. Both experiments consisted of either 2048 or 4096 T_2 and 512 or 750 T_1 data points and utilized time-proportional phase incrementation (22) to achieve phase sensitivity in ω_1. Heteronuclear multiple-quantum coherence (23) spectra were recorded in 100% ^2H_2O with 2048 T_2 and 256 or 300 T_1 data points, using hybrid states/time-proportional phase incrementation phase cycling (24) to obtain phase-sensitive spectra. All experiments were recorded at 288°, 298°, and 303°K. Amide protons were characterized as either slowly or very slowly exchanging, based on the presence of corresponding cross-peaks in sequentially acquired total correlated spectroscopy (total acquisition time, 2 hr) and NOESY spectra (total acquisition time, 24 hr) of samples freshly dissolved in ^2H_2O. Coupling constants were measured directly from resolution-enhanced one-dimensional spectra recorded in H_2O.

Structure calculations. Cross-peaks in the NOESY spectra were classified as strong, medium, or weak, and corresponding internuclear upper bound distances of 2.5, 3.5, or 5.0 Å, respectively, were assigned to each interaction. Backbone ϕ angles were constrained based on observed NOE and $^3J_{HN,H\alpha}$ coupling patterns (see below). Structures were generated using NMR-derived restraints as input to a distance geometry/simulated annealing algorithm, DGII (25), without tetrangle

bounds smoothing, using a four-dimensional embedded algorithm and an initial energy of 1024 kcal for the simulated annealing stage. Structures were considered acceptable and subjected to conjugate gradient energy minimization if the final error function was ≤1 after simulated annealing.

Results

Structure of ω-Aga-IVB. Liquid chromatography fractionation of *A. aperta* venom on a Brownlee C_8 wide-pore analytical column (see Materials and Methods) yielded multiple fractions that inhibited potassium-induced $^{45}Ca^{2+}$ entry into rat brain synaptosomes. One of the constituents in these inhibitory fractions is ω-Aga-IVA (16, 17). We subsequently focused on another fraction, which also inhibited synaptosomal Ca^{2+} entry under the same conditions (Fig. 1A). The inhibitory activity of this fraction was abolished after trypsin exposure, indicating its likely peptidergic nature. After additional purification (see Materials and Methods), the material was analyzed by ES-MS. The spectrum exhibited a series of multiply charged ions that deconvoluted to a molecular mass of 5274 Da. Amino acid composition analysis of the native peptide gave the following molar ratios of amino acids (with values from subsequent sequence analysis in parentheses): Asx, 4.4 (4); Glx, 4.4 (4); Ser, 2.6 (2); Gly, 6.6 (6); Arg, 4.5 (4); Thr, 3.8 (4); Ala, 2.6 (2); Pro, 2.1 (2); Tyr, 0.85 (1); Met, 1.0 (2); Ile, 2.9 (3); Leu, 2.1 (2); Phe, 1.1 (1); Lys, 2.0 (2). Tryptophan and cysteine were not quantified by composition analysis, but their presence was indicated by 1) a characteristic tryptophan-like UV absorbance spectrum and 2) alkylation of the reduced peptide by 4-vinylpyridine. We also noted that, whereas the native peptide was relatively resistant to trypsin digestion, reduction followed by trypsin treatment produced a complex peptide map.

Amino-terminal Edman sequencing of the reduced pyridylethylated peptide was successful through residue 43 (Fig. 1C) and indicated the presence of methionine residues at positions 29 and 42. Subsequent cyanogen bromide cleavage yielded several fragments. Amino acid composition and sequence analyses performed on two of these fragments showed them to correspond to residues 1–28 and 30–42 of the sequence previously determined by amino-terminal sequencing. A third fragment was isolated and analyzed by FAB-MS. Its molecular mass (MH^+ = 623.34 Da), when added to those of fragments 1–28 and 29–42, yielded the mass (5274 Da) established previously for the native peptide. Initial attempts to sequence this fragment were unsuccessful, due to high levels of wash-out between sequencing cycles. Subsequent covalent attachment of the carboxyl terminus of the peptide to the Sequelon filter, using carbodiimide, eliminated this problem and permitted determination of the sequence as EGLSFA.

ES-MS analysis was performed on each of the three cyanogen bromide fragments. The following values, each rounded to the nearest integer, were obtained (theoretical mass of each unprotonated fragment in parentheses): fragment 1–29, 3827 (3823.7); fragment 30–42, 1614 (1611.8); fragment 43–48, 624 (622.30). The MH^+ peak (mass, 623.34) for fragment 43–48 obtained by FAB-MS indicated that the peptide possesses a free carboxyl terminus (theoretical MH^+ mass, 623.30). Taken together, these data are consistent with the amino sequence for ω-Aga-IVB depicted in Fig. 1A, i.e., an unblocked 48-amino acid peptide with four cystines. The concentration of ω-Aga-IVB in crude venom was estimated to be 1 mM, which is approximately 10 times higher than that reported previously for ω-Aga-IVA (16).

Pharmacological properties of ω-Aga-IVB. ω-Aga-IVB blocked potassium-stimulated $^{45}Ca^{2+}$ entry into rat brain synaptosomes at low nanomolar concentrations. The concentration-dependent inhibition (Fig. 1B) was maximal at about 60% of the total response, with an estimated IC_{50} of 20 nM. The results of experiments performed in parallel with ω-Aga-IVA showed that the two peptides were virtually identical in potency and efficacy as inhibitors of rat brain synaptosomal calcium flux.

In voltage-clamp experiments, ω-Aga-IVB was found to be a potent antagonist of the high-threshold calcium channel current recorded from isolated rat cerebellar Purkinje neurons (Fig. 2). An average of ~90% of this current is carried through P-type calcium channels (15, 17). ω-Aga-IVB at concentrations of 100–800 nM blocked 90–100% of the high-threshold current. When ω-Aga-IVB was applied at 800 nM, block developed with an exponential time course (Fig. 2A), with an average time constant of 26 ± 3 sec (n = 12). Block was slower at lower toxin concentrations, with a time constant of 156 sec in an experiment with 100 nM ω-Aga-IVB. Block of P-type calcium channels was complete at all membrane potentials (Fig. 2B). In most experiments, toxin was applied while calcium channels were activated every 7–12 sec by 30-msec depolarizations to

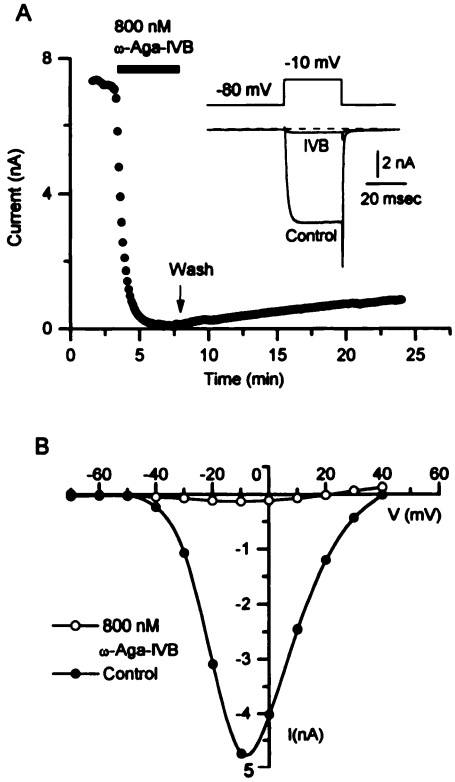

Fig. 2. Block of high-threshold calcium channel current in cerebellar Purkinje neurons. A, Block by 800 nM ω-Aga-IVB and slow recovery after wash-out. Current was elicited by 30-msec depolarizations to −10 mV, delivered from the holding potential of −80 mV every 12 sec. Current was exclusively slowly decaying, high-threshold current, and inward current (*inset*) was measured after correction for linear leak and capacity currents. B, Current-voltage relationship for calcium channel current in a Purkinje neuron before and after exposure to 800 nM ω-Aga-IVB (*IVB*). Current was blocked nearly completely at all test potentials between −40 and +40 mV. The very small remaining currents are consistent with small components of L-type and N-type current.

−10 mV; however, channel activation was not necessary for toxin binding, because equivalent block was seen in experiments in which toxin was applied to the bath during a pause in test voltage steps.

Current recovered very slowly when toxin was washed out during the usual stimulation protocol (holding potential of −80 mV, with 30-msec steps to −10 mV delivered every 7–12 sec). In the typical example shown in Fig. 2A, <20% of the control current recovered during about 15 min in toxin-free solution. Recovery could be dramatically accelerated by short voltage steps to very positive potentials. Fig. 3A shows an example in which, after a small amount of recovery in 10 min of washing, complete recovery followed a train of five voltage steps to +120 mV (30 msec each, delivered at 10 Hz). If large depolarizing voltage steps were given in the presence of toxin, recovery was followed by re-block occurring with a time course similar to that observed during the original application of the toxin (Fig. 3B).

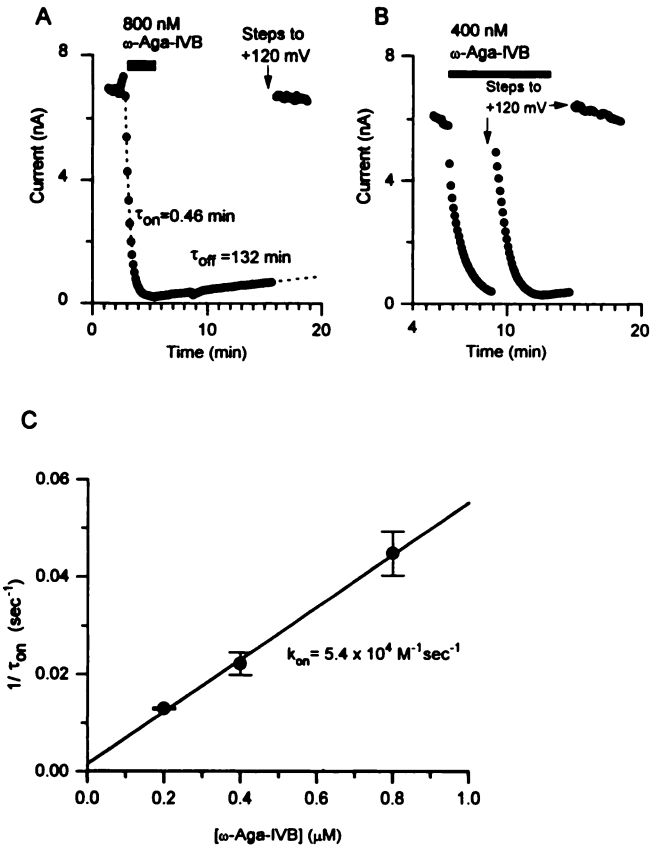

Fig. 3. Concentration-dependent block and voltage-dependent unblock of P-type current in Purkinje neurons. A, Time course of block by 800 nM ω-Aga-IVB and speeding of recovery by strong depolarizations. After application of 800 nM ω-Aga-IVB for about 3 min, toxin-free solution was applied for 10 min while test pulses (30-msec pulses to −10 mV, from a holding potential of −80 mV) were delivered every 6 sec. At the point marked by the *arrow*, a series of five steps to +120 mV (50-msec each) were delivered at 10 Hz, resulting in complete recovery of the current elicited by the next test pulse to −10 mV. *Dashed line* during onset of block is the best fit of a single-exponential function with a time constant of 0.46 min. *Dashed line* during slow recovery from block is the best fit of a single-exponential function (time constant of 132 min) assuming eventual recovery to 7 nA, the size of the current after the depolarizing steps. B, Voltage steps to +120 mV (a series of five 50-msec steps, delivered at 10 Hz) in the continuous presence of 400 nM ω-Aga-IVB, resulting in transient relief of block followed by reblock. C, Reciprocal of the time constant for development of block versus toxin concentration. *Points*, mean values of determinations in multiple cells (n = 3 for 200 nM, n = 8 for 400 nM, and n = 12 for 800 nM). *Error bars*, standard errors.

It was difficult to determine directly the half-blocking concentration of ω-Aga-IVB. In one experiment, 100 nM toxin produced nearly complete block, suggesting a half-blocking concentration at least 10 times lower. Unfortunately, block by concentrations below 100 nM was too slow to be accurately separated from run-down of the current that occurred in the absence of toxin. However, because both development and reversal of block occurred with kinetics consistent with 1:1 binding of toxin to channel, we were able to estimate the equilibrium constant for binding (K_d) from the kinetic data. The development of block could be fit well by a single-exponential function over a range of toxin concentrations, and the time constant (τ_{on}) was inversely proportional to toxin concentration, as expected for 1:1 binding. The values of $1/\tau_{on}$ versus toxin concentration (Fig. 3C) could be well fit by a line corresponding to a rate constant for toxin binding (k_{on}) of 5×10^4 M^{-1} sec^{-1}. The rate constant for toxin unbinding was estimated by fitting an exponential function to the recovery occurring in a 10–15-min period after removal of toxin (taking as asymptote either the current before application of toxin or the current after a train of depolarizations, as in Fig. 3A). Values of τ_{off} at the holding potential (−80 mV) ranged from 70 to 150 min, with an average value of 113 ± 11.4 min (n = 12). The unbinding rate constant (k_{off}) corresponding to this value ($1/\tau_{off}$) was 1.5×10^{-4} sec^{-1}. Using these rate constants, the K_d for block of P-type channels by ω-Aga-IVB was estimated as 3 nM.

Selectivity of Ca^{2+} channel block by ω-Aga-IVB. We also tested the activity of ω-Aga-IVB against other types of calcium channels in various rat neurons. A subpopulation of cerebellar Purkinje neurons possess a low-threshold T-type current, manifested as a transient component of current on top of the more slowly decaying P-type current (15, 26). Fig. 4A shows currents from such a Purkinje neuron. ω-Aga-IVB at 200 nM selectively inhibited the P-type current, leaving the transient T-type current (Fig. 4A, *left*). T-type current is also manifested as a slowly decaying tail current upon repolarization, 1 order of magnitude slower than tail currents through P-type channels. This slow component of tail current was unaffected by ω-Aga-IVB (Fig. 4A, *right*).

Identified currents through L-type calcium channels are conveniently obtained using the dihydropyridine agonist Bay K8644, which enhances L-type current (9, 27) and dramatically slows tail currents through L-type channels (12, 28). Fig. 4B shows records from a DRG neuron in which 3 μM Bay K8644 produced a slowly decaying tail current in a neuron first treated with 3 μM ω-CgTX to eliminate N-type current. Application of 200 nM ω-Aga-IVB (in the continuing presence of ω-CgTX and Bay K8644) had no effect on the Bay K8644-enhanced tail current, showing the lack of activity against L-type calcium channels. (The toxin did inhibit the current during the test pulse to −20 mV by about 20% and inhibited a rapid component of tail current, showing activity against other components of total calcium current in DRG neurons.) The lack of activity of 200 nM ω-Aga-IVB on Bay K8644-enhanced L-type current was found in five of five rat DRG neurons in which L-type current was enhanced by 3 μM Bay K8644.

The effect of ω-Aga-IVB on N-type calcium channels was investigated in rat sympathetic neurons (superior cervical ganglion), in which most of the high-threshold current is ω-CgTX-

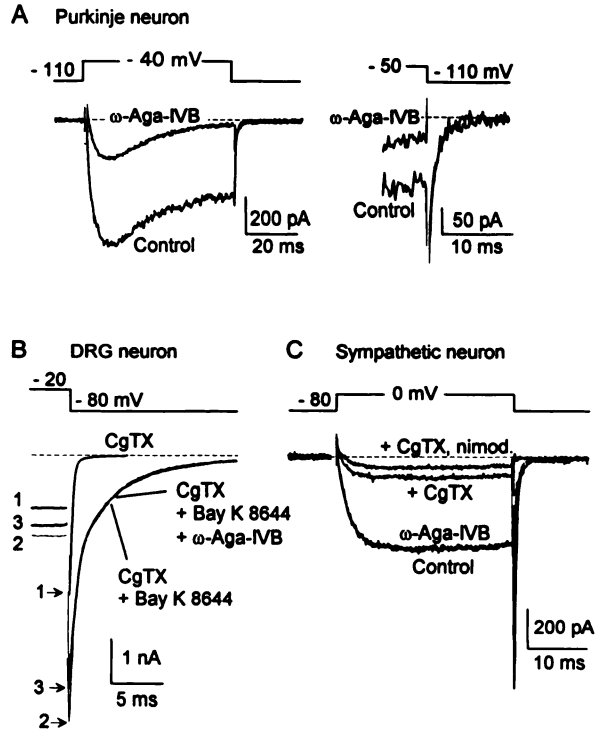

Fig. 4. Lack of effect of ω-Aga-IVB on T-type, L-type, and N-type calcium currents. A, ω-Aga-IVB block of P-type but not T-type current in a cerebellar Purkinje neuron. Effect of 200 nM ω-Aga-IVB on current elicited by a 60-msec depolarization from −110 mV to −40 mV (*left*) and on tail current after a depolarization to −50 mV that elicited predominantly low-threshold T-type current (*right*). B, Lack of effect of ω-Aga-IVB on Bay K8644-enhanced L-type current in a rat DRG neuron. Current was elicited by 60-msec depolarization applied from −80 to −20 mV. The figure focuses on deactivating tail currents recorded upon repolarization to −80 mV in the presence of 3 μM ω-CgTX (*trace 1*), after addition of 3 μM Bay K8644 in the continuing presence of ω-CgTX (*trace 2*), and after addition of 200 nM ω-Aga-IVB, with both ω-CgTX and Bay K8644 still present (*trace 3*). C, Lack of effect of ω-Aga-IVB on N-type or L-type current in a rat sympathetic neuron. Current was elicited by a 30-msec depolarization from −80 to 0 mV in control, after addition of 200 nM ω-Aga-IVB, after subsequent addition of 5 μM ω-CgTX (with ω-Aga-IVB still present), and after subsequent addition of 3 μM nimodipine (in the continuing presence of 200 nM ω-Aga-IVB and 5 μM ω-CgTX).

sensitive N-type current. In each of six sympathetic neurons, 200–400 nM ω-Aga-IVB had no significant effect on the overall current. In three cells with stable control currents, currents obtained under control conditions and after addition of 200 nM ω-Aga-IVB were identical (e.g., see Fig. 4C). In three other cells, a small current reduction produced by 200–400 nM ω-Aga-IVB was not distinguishable from run-down of control currents.

These results show that ω-Aga-IVB is a highly selective blocker of P-type channels, with no effect on T-type, L-type, or N-type calcium channels. ω-Aga-IVA has a similar profile of selectivity (17). Some neurons, including rat spinal cord neurons, have a complex mixture of channels contributing to the overall high-threshold current, including L-type, N-type, P-type, and other, unidenitifed, channels (17). The similarity in selectivity between ω-Aga-IVB and ω-Aga-IVA was tested more rigorously by examining overlap in block by these two toxins in spinal cord neurons. Examples are shown in Fig. 5. In the experiment of Fig. 5A, ω-Aga-IVA had no additional effect on a cell in which ω-Aga-IVB had blocked a component of the current. As shown in Fig. 5B, the same result was obtained

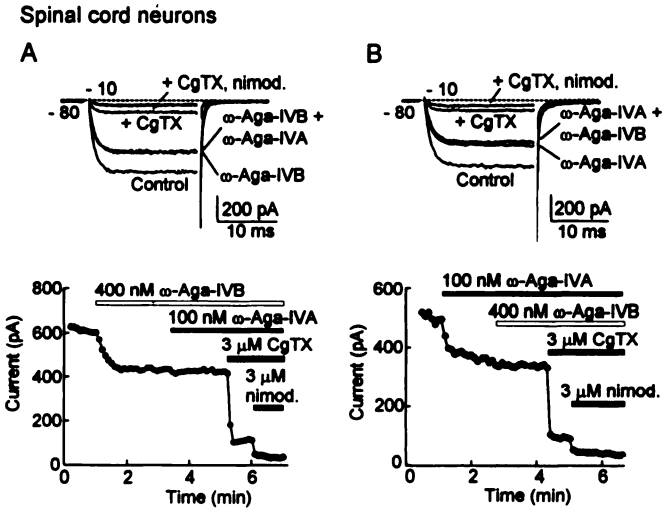

Fig. 5. ω-Aga-IVB targets the same component of current in spinal cord neurons as does ω-Aga-IVA. A, *Upper*, ω-Aga-IVB blocks a fraction of high-threshold current and occludes block by ω-Aga-IVA in a spinal cord neuron. Current was elicited by 30-msec depolarizations applied every 6 sec from −80 mV to −10 mV. Records corrected for leak and capacity currents are shown in control, after application of 400 nM ω-Aga-IVB, with both ω-Aga-IVB and 100 nM ω-Aga-IVA, and with subsequent addition of 3 μM ω-CgTX and then 3 μM nimodipine (*nimod.*) (in the continuing presence of the other blockers). *Lower*, time course of the peak current in the same experiment. B, *Upper*, Occlusion by ω-Aga-IVA of the blocking effect of ω-Aga-IVB in another spinal cord neuron. Same protocol as in A, except that 100 nM ω-Aga-IVA was applied first, followed by 400 nM ω-Aga-IVB, 3 μM ω-CgTX, and 3 μM nimodipine. *Lower*, time course of the peak current.

from another cell when ω-Aga-IVA and ω-Aga-IVB were applied in the reverse order. Complete occlusion between the effects of the two toxins was seen in each of five cells examined (three with ω-Aga-IVA applied first and two with ω-Aga-IVB applied first).

NMR analysis of ω-Aga-IVB. Complete proton assignments of all 48 amino acids in ω-Aga-IVB were determined using conventional two-dimensional NMR sequential assignment techniques (29). These results confirmed the sequence determined by Edman degradation and provided a basis for subsequent experiments. Notably, the chemical shifts of residues 39–48 occurred near values expected for random coil peptides, consistent with little ordered structure in this region of the molecule. The distribution of observed NOEs is summarized in Fig. 6, with the largest number being concentrated among residues 4–36, suggesting a high degree of cross-linking via cysteines. Preliminary analysis of the data suggested the presence of a small, three-stranded, antiparallel β-sheet composed of residues 10–12, 25–27, and 34–36. First, Hα-Hα, Hα-HN, and HN-HN interstrand NOEs were observed. Second, all of the very slowly exchanging NH signals appeared in this region, consistent with interstrand hydrogen bonding. Third, many α carbon resonances were shifted downfield for most of these residues (30).

For structure calculations, 267 interproton distances (135 long range) from NOEs and three ϕ (residues 6, 32, and 37) plus seven χ_1 dihedral angles derived from coupling constants (31) were used as restraints for input into DGII. The seven χ_1 angles were constrained based on observed NOE and J coupling patterns, as follows: Cys-4 and Cys-12, 40–80°; Cys-19, Cys-20, Cys-34, and Cys-36, −40 to −80°; Cys-25, −160 to 160°. The χ_1

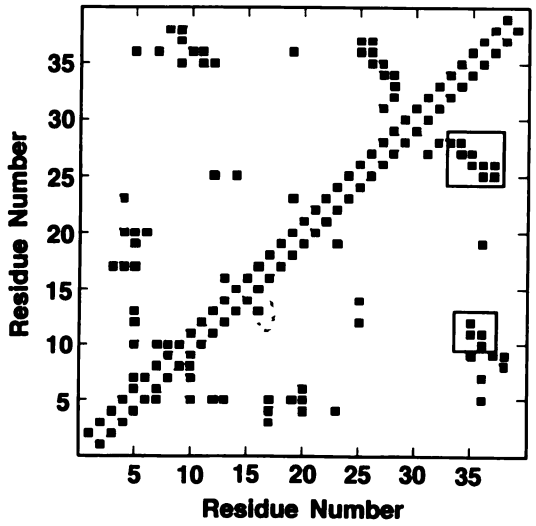

Fig. 6. Inter-residue NOEs used as restraints in DGII calculations on ω-Aga-IVB. Off-diagonal points at (*x*, *y*) indicate one or more NOEs observed between residues *x* and *y*. *Boxed areas*, interstrand NOEs arising from the three-stranded β-sheet.

angle for Cys-27 could not be determined. Six additional hydrogen bond restraints, between residues 10 and 36, 26 and 35, 37 and 24, and 12 and 34, were inferred from slow amide exchange within the β-sheet substructure described above. An initial structure with extended conformation was constructed, and 10 structures were generated using the NMR-derived restraints. In an effort to establish the disulfide bonding pattern, the close contacts between cystine β carbons were analyzed. Of the 10 structures, cysteine Cβ-Cβ distances of <3 Å were observed between the following cysteine pairs with the indicated frequency: 4–20, 12–25, and 27–34 in all cases, 19–36 in seven cases, 19–25 in four cases, and 12–36 in one case. Because the disulfide bonds involving cysteines 12, 19, 25, and 36 were ambiguous from these preliminary calculations, three separate molecules were built incorporating the three remaining possible disulfide bonds, as follows: **1**, 4–20, 19–25, 12–36, and 27–34; **2**, 4–20, 12–19, 25–36, and 27–34; **3**, 4–20, 12–25, 19–36, and 27–34.

These were used as starting structures for additional DGII calculations. Using identical constraints, average final errors of 1.14, 5.47, and 0.76 were obtained for starting structures **1**, **2**, and **3**, respectively (25). Taking these results together with the preliminary statistical analysis of the initial calculations, which included no disulfide contraints, it can be concluded that the disulfide bonding pattern in ω-Aga-IVB is as shown in structure **3** (above) and in Fig. 7. Furthermore, pattern **2** would result in two dislocated double loops separated by an RGRP sequence and would be expected to undergo more extensive fragmentation than was observed upon trypsin treatment of ω-Aga-IVB (see above). It is noteworthy that, although the data are most consistent with pattern **3**, the overall topology of amino acids is quite similar among the refined structures resulting from all three sets of calculations. Efforts to map the disulfide bond configuration using tryptic digestion and MS have thus far not been successful, presumably due to hindering of enzyme access in the cystine-rich portion of the molecule.

Using a randomly selected starting conformation with disulfide bonds between cystines 4–20, 12–25, 19–36, and 27–34 as input for additional DGII calculations, 34 of 50 structures converged and were used for RMS deviation analysis. The Cα carbons for residues 3–37 were superimposed with an average RMS deviation of 2.2 Å. Residues 39–48 are extremely unordered, consistent with the observed chemical shifts and lack of long-range NOEs observed in this region. When the Cα carbons for residues 10–12, 25–27, and 34–36 were used to compare the structures, a much tighter RMS deviation of 1.3 Å was observed among these atoms. These residues comprise the β-sheet and have a relatively larger number of experimental restraints per residue. When the NMR observations are taken together, a picture emerges for ω-Aga-IVB that consists of a group of relatively rigid "core" amino acids, four flexible loop regions, and an extremely flexible carboxyl-terminal tail. In the globular portion of the peptide, a large number of positively charged residues are clustered on one face of the molecule (Fig. 7). Significantly, many of these basic side chains are conserved between ω-Aga-IVA and ω-Aga-IVB.

Discussion

ω-Aga-IVB is the second antagonist of P-type Ca^{2+} channels identified from *A. aperta* spider venom. It is closely related in size (48 amino acids) to ω-Aga-IVA (16), shows identical placement of the cysteine residues, and has overall sequence identity of 73%. These data suggest that the disulfide bonding patterns of the two molecules are likely to be very similar. However, whereas ω-Aga-IVA is a highly basic molecule (10 positively charged and three negatively charged residues), ω-Aga-IVB is not (six positively charged and six negatively charged residues).

With such a large difference in the overall charge of the peptides, we had expected that ω-Aga-IVB might interact with calcium channels somewhat differently than does ω-Aga-IVA, especially because the unbinding of ω-Aga-IVA is strongly voltage dependent (17). In fact, however, the calcium channel-blocking properties of the two molecules are remarkably similar. Both are highly selective for blocking P-type calcium channels, with no blocking activity against T-type, L-type, or N-type channels. The estimated K_d of 3 nM for ω-Aga-IVB block of P-type channels is quite similar to that of 2 nM previously estimated for ω-Aga-IVA (17). And, as shown for ω-Aga-IVA, the unbinding reaction of ω-Aga-IVB is dramatically accelerated by depolarization of the membrane, increasing >1000-fold at +120 mV, compared with −80 mV. The two molecules must interact with the high affinity binding site on the P-type calcium channel in very similar manners. The only difference in channel-blocking activity is that block by ω-Aga-IVB develops more slowly (~8-fold) than does that by ω-Aga-IVA and also reverses more slowly during wash-out using normal stimulation protocols. From a biological perspective, it is interesting that, because ω-Aga-IVB is present in venom at a 10-fold higher concentration, the rates of block by ω-Aga-IVB and ω-Aga-IVA upon venom injection might be quite similar.

The similar K_d values for block of P-type calcium channels by the two toxins measured electrophysiologically fit well with their similar, albeit lower, potencies against potassium-stimulated calcium flux in synaptosomes (IC_{50}, ~20 nM). This apparent potency difference may result partly from a nonlinearity between calcium conductance and accumulated calcium and partly from the depolarized conditions characteristic of potassium stimulation in the synaptosome experiments, where the

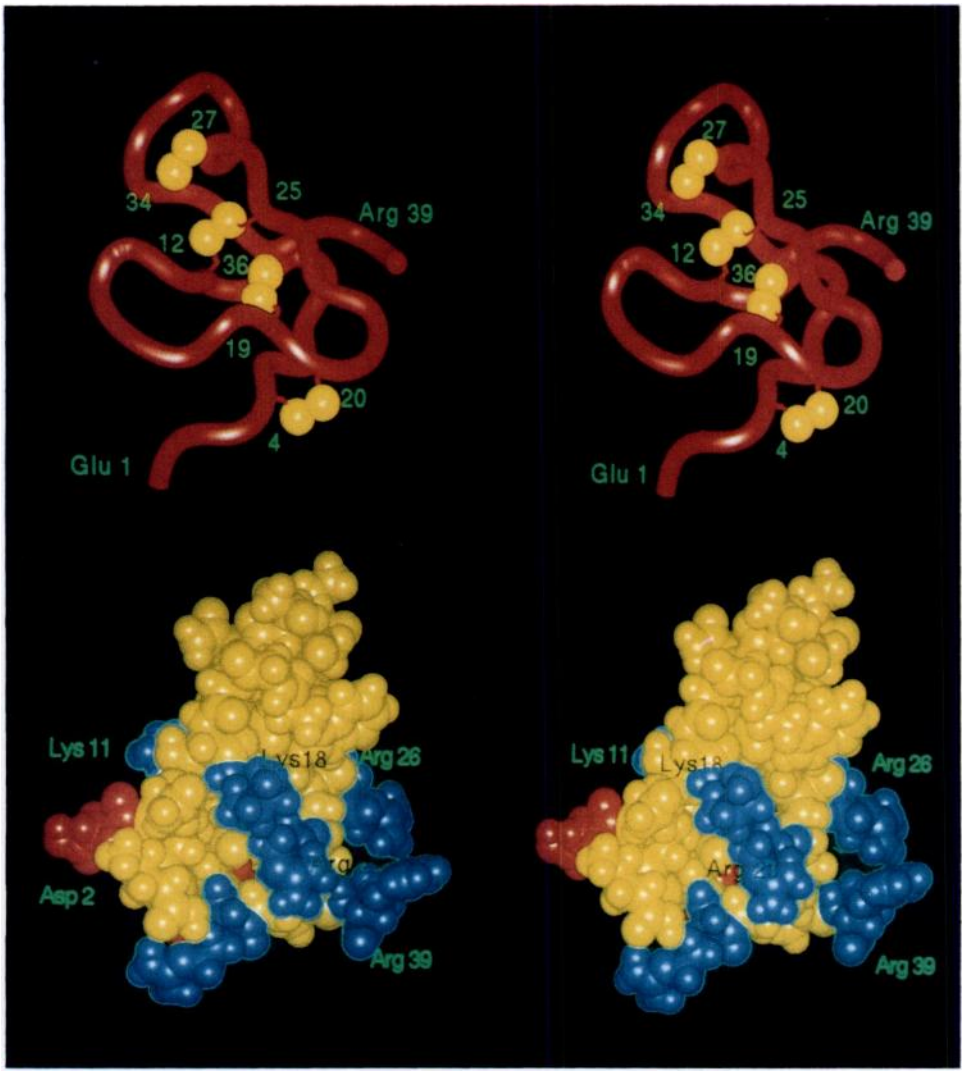

Fig. 7. Relaxed stereo views of three-dimensional structural features of ω-Aga-IVB. Only residues 1–39 are shown. *Upper*, ribbon diagram showing the overall backbone fold and locations of the disulfides. *Lower*, Space-filling model showing the topological positive (*blue*) and negative (*red*) charge distribution in ω-Aga-IVB. The blue-colored residue at the bottom of the space-filling model is Arg 21.

rate of toxin unbinding may be accelerated, compared with that at normal resting potentials.

Although the primary structures of the two toxins are quite similar overall, the amino termini of the peptides are very different. Amino-terminal amino acids of ω-Aga-IVB are predominantly acidic amino acids, whereas this region in ω-Aga-IVA is quite basic (Fig. 1). This region of the molecule is apparently not important for binding.

It is intriguing that clusters of basic residues occur at similar locations, between positions 10 and 27, in both toxins. The NMR results for ω-Aga-IVB suggest that these positively charged groups are clustered on the same face of the toxin. It is tempting to think that this face of the molecule interacts with the calcium channel.

The NMR data for ω-Aga-IVB allow definition of a low-resolution structure sufficient to define a unique disulfide bonding pattern. Because the placements of cysteine residues in ω-Aga-IVB and ω-Aga-IVA are identical, we now have a working model for the cystine configuration in both molecules. The pattern established here is strikingly similar to those of other cysteine-rich peptide toxins, such as the μ-agatoxins (32) and ω-conotoxins (33). Thus, cystines 4–20 and 19–36 of ω-Aga-IVB are spaced in a manner similar to that of those occurring in μ-Aga-V and ω-CgTX. Despite these similarities in secondary structure, these toxins have very diverse properties. It will be interesting to construct systematically altered analogs of ω-Aga-IVB and ω-CgTX to determine which portions of the molecules determine selectivity for P-type versus N-type calcium channels.

References

1. Olivera, B. M., J. Rivier, C. Clark, C. A. Ramilo, G. P. Corpuz, F. C. Abogadie, E. E. Mena, S. R. Woodward, D. R. Hillyard, and L. J. Cruz. Diversity of *Conus* neuropeptides. *Science (Washington D. C.)* **249**:257–263 (1990).
2. Olivera, B. M., J. S. Imperial, L. J. Cruz, V. P. Bindokas, V. J. Venema, and M. E. Adams. Calcium channel-targeted polypeptide toxins. *Ann. N. Y. Acad. Sci.* **635**:114–122 (1991).
3. Dolly, J. O., ed. *Neurotoxins in Neurochemistry*. John Wiley & Sons, New York (1988).
4. Adams, M. E., V. P. Bindokas, L. Hasegawa, and V. J. Venema. *omega*-Agatoxins: novel calcium channel antagonists of two subtypes from funnel web spider (*Agelenopsis aperta*) venom. *J. Biol. Chem.* **265**:861–867 (1990).
5. Hess, P. Calcium channels in vertebrate cells. *Annu. Rev. Neurosci.* **13**:337–356 (1990).
6. Tsien, R. W., P. T. Ellinor, and W. A. Horne. Molecular diversity of voltage-dependent Ca^{2+} channels. *Trends Pharmacol. Sci.* **12**:349–354 (1991).
7. Miller, R. J. Voltage sensitive Ca^{2+} channels. *J. Biol. Chem.* **267**:1403–1406 (1992).
8. Snutch, T. P., and P. B. Reiner. Ca^{2+} channels: diversity of form and function. *Curr. Opin. Neurobiol.* **2**:247–253 (1992).
9. Nowycky, M. C., A. P. Fox, and R. W. Tsien. Long-opening mode of gating of neuronal calcium channels and its promotion by the dihydropyridine calcium agonist Bay K 8644. *Proc. Natl. Acad. Sci. USA* **82**:2178–2182 (1985).

10. Aosaki, T., and H. Kasai. Characterization of two kinds of high-voltage-activated Ca-channel currents in chick sensory neurons: differential sensitivity to dihydropyridines and *omega*-conotoxin GVIA. *Pflügers Arch.* **414**:150–156 (1989).
11. Williams, M. E., D. H. Feldman, A. F. McCue, R. Brenner, G. Velicelebi, G. B. Ellis, and M. M. Harpold. Structure and function of $\alpha 1$, $\alpha 2$, and β subunits of a novel human neuronal calcium channel subtype. *Neuron* **8**:71–84 (1992).
12. Plummer, M. R., D. E. Logothetis, and P. Hess. Elementary properties and pharmacological sensitivities of calcium channels in mammalian peripheral neurons. *Neuron* **2**:1453–1463 (1989).
13. Williams, M. E., P. F. Brust, D. H. Feldman, P. Saraswathi, S. Simerson, A. Maoufi, A. F. McCue, G. Velicelebi, S. B. Ellis, and M. M. Harpold. Structure and functional expression of an ω-conotoxin-sensitive human N-type calcium channel. *Science (Washington D. C.)* **257**:389–395 (1992).
14. Llinas, R., M. Sugimori, J. W. Lin, and B. Cherksey. Blocking and isolation of a calcium channel from neurons in mammals and cephalopods utilizing a toxin fraction (FTX) from funnel-web spider poison. *Proc. Natl. Acad. Sci. USA* **86**:1689–1693 (1989).
15. Regan, L. J. Voltage-dependent calcium currents in Purkinje cells from rat cerebellar vermis. *J. Neurosci.* **11**:2259–2269 (1991).
16. Mintz, I. M., V. J. Venema, K. M. Swiderek, T. D. Lee, B. P. Bean, and M. E. Adams. P-type calcium channels blocked by the spider toxin, ω-Aga-IVA. *Nature (Lond.)* **355**:827–829 (1992).
17. Mintz, I. M., M. E. Adams, and B. P. Bean. P-type calcium channels in rat central and peripheral neurons. *Neuron* **9**:85–95 (1992).
18. Venema, V. J., K. M. Swiderek, T. D. Lee, G. M. Hathaway, and M. E. Adams. Antagonism of synaptosomal calcium channels by subtypes of ω-agatoxins. *J. Biol. Chem.* **267**:2610–2615 (1992).
19. Braunschweiler, L., and R. R. Ernst. Coherence transfer by isotropic mixing: application to proton correlation spectroscopy. *J. Magn. Reson.* **53**:521–528 (1983).
20. Bax, A., and D. G. Davis. MLEV-17-based two dimensional homonuclear magnetization transfer spectroscopy. *J. Magn. Reson.* **65**:355–360 (1985).
21. Kumar, A., R. R. Ernst, and K. Wüthrich. A two-dimensional nuclear Overhauser enhancement (2D NOE) experiment for the elucidation of complete proton-proton cross-relaxation networks in biological macromolecules. *Biochem. Biophys. Res. Commun.* **95**:1–6 (1980).
22. Marion, D., and K. Wüthrich. Application of phase sensitive two-dimensional correlated spectroscopy (COSY) for measurements of spin-spin coupling constants in proteins. *Biochem. Biophys. Res. Commun.* **113**:967–974 (1983).
23. Bax, A., R. H. Griffey, and B. L. Hawkins. Correlation of proton and nitrogen-15 chemical shifts by multiple quantum NMR. *J. Magn. Reson.* **55**:301–315 (1983).
24. Marion, D., M. Ikura, R. Tschudin, and A. Bax. Rapid recording of 2D NMR spectra without phase cycling: application to the study of hydrogen exchange in proteins. *J. Magn. Reson.* **85**:393–399 (1989).
25. Havel, T. F. An evaluation of computational strategies for use in the determination of protein structure from distance constraints obtained by nuclear magnetic resonance. *Prog. Biophys. Mol. Biol.* **56**:43–78 (1991).
26. Kaneda, M., M. Wakamori, C. Ito, and N. Akaike. Low-threshold calcium current in isolated Purkinje cell bodies of rat cerebellum. *J. Neurophysiol.* **63**:1046–1051 (1990)
27. Hess, P., J. B. Lansman, and R. W. Tsien. Different modes of gating behavior favored by dihydropyridine Ca agonists and antagonists. *Nature (Lond.)* **311**:538–544 (1984).
28. Regan, L. J., D. W. Sah, and B. P. Bean. Ca^{2+} channels in rat central and peripheral neurons: high-threshold current resistant to dihydropyridine blockers and *omega*-conotoxin. *Neuron* **6**:269–280 (1991).
29. Wüthrich, K. *NMR of Proteins and Nucleic Acids.* J. Wiley and Sons, New York (1986).
30. Spera, S., and A. Bax. Empirical correlation between protein backbone conformation and Cα and Cβ ^{13}C nuclear magnetic resonance chemical shifts. *J. Am. Chem. Soc.* **113**:5490–5492 (1991).
31. Clore, G. M., P. T. Wingfield, and A. M. Gronenborn. High resolution three-dimensional structure of interleukin 1β in solution by three- and four-dimensional nuclear magnetic resonance spectroscopy. *Biochemistry* **30**:2315–2323 (1991).
32. Skinner, W. S., M. E. Adams, G. B. Quistad, H. Kataoka, B. J. Cesarin, F. E. Enderlin, and D. A. Schooley. Purification and characterization of two classes of neurotoxins from the funnel web spider, *Agelenopsis aperta*. *J. Biol. Chem.* **264**:2150–2155 (1989).
33. Olivera, B. M., D. R. Hillyard, J. Rivier, S. R. Woodward, G. Corpuz, and L. J. Cruz. Conotoxins: targeted peptide ligands from snail venoms. *Am. Chem. Soc. Symp. Ser.* **418**:256–278 (1990).

Send reprint requests to: Michael E. Adams, Department of Entomology, University of California, Riverside, CA 92521.